

# Study of the Villin Headpiece folding dynamics by combining coarse-grained Monte Carlo evolution and all-atom Molecular Dynamics

Giacomo M. S. De Mori<sup>1</sup> Giorgio Colombo<sup>1</sup> and Cristian Micheletti<sup>2</sup>

<sup>1</sup> Istituto di Chimica del Riconoscimento Molecolare, CNR, Via Mario Bianco 9, 20131 Milano, Italy

<sup>2</sup> International School for Advanced Studies (S.I.S.S.A.) and INFN, Via Beirut 2-4, 34014 Trieste, Italy

(Dated: March 23, 2022)

The folding mechanism of the Villin headpiece (HP36) is studied by means of a novel approach which entails an initial coarse-grained Monte Carlo (MC) scheme followed by all-atom molecular dynamics (MD) simulations in explicit solvent. The MC evolution occurs in a simplified free-energy landscape and allows an efficient selection of marginally-compact structures which are taken as viable initial conformations for the MD. The coarse-grained MC structural representation is connected to the one with atomic resolution through a “fine-graining” reconstruction algorithm. This two-stage strategy is used to select and follow the dynamics of seven different unrelated conformations of HP36. In a notable case the MD trajectory rapidly evolves towards the folded state, yielding a typical RMS deviation of the core region of only 2.4Å from the closest NMR model (the typical RMSD over the whole structure being 4.0Å). The analysis of the various MC-MD trajectories provides valuable insight into the details of the folding and mis-folding mechanisms and particularly about the delicate influence of local and non-local interactions in steering the folding process.

## Introduction

The characterization of the process by which proteins fold into their native structures is at the heart of molecular biology. Starting from the pioneering work of Anfinsen, several experimental studies in the past decades have provided support for the fact that the knowledge of the mere primary sequence ought to allow the prediction of the native structure for a large class of proteins [1, 2, 3, 4, 5]. This conclusion relies on the notion that, under physiological conditions, the native conformation is at a minimum of a multidimensional free-energy landscape [1, 2, 6, 7, 8, 9, 10]. Furthermore, the fact that several proteins are known to reach the native configuration from a variety of initial configurations has been rationalized in the assumption that, through natural evolution, the free-energy profile around the native minimum is relatively smooth and with a wide basin of attraction in configuration space [8, 11, 12, 13].

These facts open, in principle, the possibility to predict the native state of proteins through a numerical simulation of the dynamical evolution of an arbitrary initial (“unfolded”) conformation. The feasibility of this scheme would have profound ramifications both from the theoretical and practical point of view. Though there is an ongoing progress in this direction [14, 15, 16, 17], present computational techniques and resources are not adequate to follow the folding dynamics of a medium-size protein (e.g. 100 residues) in its surrounding solvent for time intervals comparable to the experimental folding times [18, 19, 20, 21].

The methodology that we discuss here aims at augmenting the reach of numerical folding dynamics starting from the only knowledge of the protein sequence. The strategy exploits a two-stage simulation scheme where a protein’s dynamical evolution is first followed through a coarse-grained Monte Carlo (MC) conformational search followed by all atom molecular dynamics (MD) simulations in explicit solvent. We discuss its application to the Villin headpiece (HP36) for which we generate several independent trajectories (and reach, for the core region, residues 9–32, a root mean square deviation (RMSD) of 0.24 nm from the closest NMR model [22]).

The interest in the villin headpiece stems from the fact that, despite it consists of only 36 residues, with no cysteines, it is able to fold autonomously and rapidly (in about 10  $\mu$ s [23, 24]). Along with other short fast-folding proteins, it has been extensively investigated experimentally with the purpose of elucidating general mechanisms of the folding kinetics that ought to be transferable to longer and more complex proteins. On the other hand villin also constitutes an ideal reference case for theoretical studies, since its short length and folding rapidity allow to bridge the gap between the time scales addressable by explicit numerical dynamics and those relevant for folding [25, 26, 27, 28, 29, 30, 31].

In this respect, a notable reference study is constituted by the one of Duan and Kollman which, starting from an extended villin conformation, followed its evolution for about 1  $\mu$ s using the AMBER force field and explicit solvent [25]. It is important to remark that the explicit modeling of water molecules in the simulation introduces a number of atoms that typically greatly exceeds the ones constituting the protein itself and hence is computationally very intensive. This computational cost is rewarded by the possibility to capture the delicate, but crucial effects of the solvent-protein interactions [32].

By relaxing the accuracy of the solvent treatment it is possible to increase the MD efficiency. This approach, which usually entails the “integration” of the solvent degrees of freedom in effective inter-atomic potentials has been adopted in several simulation studies. Ferrara and Caflisch, for instance, could follow the folding pathway of a three-stranded antiparallel  $\beta$ -sheet peptide

at high temperature with MD [33]. More recently Pande and Shirts adopted the implicit solvent approximation in an innovative distributed-computing approach [34]. For the case of Villin, the numerical speed-up obtained by the simplified solvent treatment allowed to address a total time scale of the order of  $1\ \mu\text{s}$ , distributed across a large number of short trajectories each of about 30 ns. In such short simulations the choice of the starting protein structures has a profound impact on the possibility to relate the properties of the simulated system to experiments. This issue has been recently addressed by Fersht who discussed the presence of important lag-phases in all-atom MD simulations starting from random or completely extended conformations [35, 36].

Several methods and techniques have been developed over the years to overcome the time limitations of all-atom MD. A widely-used strategy is to renounce to follow the folding pathway in favor of identifying the conformations of lowest free energy through various optimization techniques including simulated annealing, multicanonical methods, genetic algorithms etc. [37, 38, 39, 40, 41, 42, 43, 44]. Another commonly employed route is to simplify not only the description of the solvent but also of the protein structure itself. Accordingly, several coarse-grained models have been introduced where the protein is described as a chain of linked beads which interact through suitable effective potentials. The drastic structural simplification entailed by these models allows to explore a portion of the conformational space vastly larger than in all-atom MD. However, the limitations of both the structural representations and of the energy functions clearly prevent from reproducing the finer features of the folding process. Nevertheless they have proved valuable for capturing and analyzing various general aspects such as the calorimetric cooperativity, the relation between native-state topology and folding rates, the identification of folding nuclei and the modeling of functional motions etc. [12, 45, 46, 47, 48, 49, 50, 51, 52, 53, 54, 55, 56]

These observations suggested the present approach which combines a coarse-grained Monte Carlo (MC) search with all atom molecular dynamics (MD) simulations in explicit solvent. The effect of the coarse-grained part is to simplify the protein's energy landscape so to identify efficiently physically-meaningful starting conformations for the MD. After bringing these structures into the realm of all-atom representations, explicit solvent MD is used to introduce back the fine chemical details which are ultimately responsible for driving the evolution towards the native state. The link between the two structural representations is a fine-graining algorithm which allows to reconstruct reliably the full atomic detail of the protein using a library of previously generated protein fragments. The scheme adopted here therefore aims at extending the reach of ordinary MD simulations by using simple physico-chemical criteria to identify the marginally-compact starting conformations in which partial formation of secondary and tertiary interactions has taken place. Thus, the approach has a different spirit from that followed in other two-stage approaches, notably the pioneering work of Vieth et al. [57] and Liwo et al. [58], where the fine-graining step was aimed at perturbing or refining the coarse-grained structures which minimized a given energy functional

## Results

The simplification of the free-energy landscape operated by the coarse-grained MC approach is achieved through a coarse-graining of the structural degrees of freedom of the protein; in particular the protein is described in terms of its  $C_\alpha$  trace and of the associated  $C_\beta$  centroids. This schematic description is accompanied by a simplification of the energy functional (see Methods) which incorporates effective pairwise interactions among amino acids, the local propensity to form secondary motifs and a term favoring the packing of the latter. Within this framework, the thermodynamics of the HP36 protein can be characterized by means of a MC evolution involving crankshaft and pivot moves. These moves preserve the length of the effective bonds joining consecutive  $C_\alpha$ 's (equal to  $3.8\text{\AA}$ ). The average energy and radius of gyration,  $R_g$  as a function of temperature of the coarse-grained system are visible in Fig. 1.

As the temperature of the system is decreased, the protein undergoes a collapse signaled by the concomitant decrease of both the radius of gyration,  $R_g$ , and the average system energy, see Fig. 1. The system density of states does not however possess the marked concavity which is distinctive of first-order transitions. This fact reflects the generality of the coarse-grained energy functional adopted here. In fact, in order to reproduce in simplified models the typical all-or-none character of folding transitions it is necessary to optimize either the protein sequence or the energy parameters [49, 59, 60, 61, 62]. In correspondence of the collapse temperature,  $T_c$ , the specific heat exhibits a peak which reflects the large energy fluctuations associated to the coexistence of rather open configurations with more globular structures (see Fig. 1). The latter ones typically possess local secondary elements (up to 1/3 of the residues are found in helical conformations) and are further compactified at lower temperatures. The protein at  $T_c$  is thus poised to collapse into compact conformations with non-trivial secondary content. Thus, the structures sampled by the MC algorithm at  $T_c$  represent attractive candidates for all-atom MD evolution for several reasons: (1) they possess good secondary content, (2) they are not unnaturally compact and (3) the conformational variability at  $T_c$  is such that significantly different structures can be picked. It is also worth to mention that another intuitive strategy would be to start the MD runs from the lowest energy states of the coarse-grained model. However, the resulting structures, once reconstructed with their atomic detail, produced steric clashes among the atoms which could not be removed by e.g. relaxing the reconstructed structure before the actual MD run. Accordingly, the lowest-energy conformations of the coarse-grained model were not used as inputs for the all-atom dynamical evolution.

Seven uncorrelated conformations were thus chosen from a MC trajectory thermalised at  $T_c$  and subject to the fine-graining reconstruction procedure described in Material and Methods. The all-atom protein models obtained were first solvated using the SPC water model and subjected to minimization in order to remove possible bad steric contacts. After equilibration, as described in Materials and Methods (section Molecular Dynamics) each model was evolved with completely unbiased MD simulations at 300 K based on the Gromos96 force field and explicit solvent. To test the viability of the force field at this temperature, and also to produce a term of reference for the other simulations we first followed the dynamical evolution of HP36 for 50 ns starting from the minimized averaged NMR model of the PDB structure 1VII. The evolution shows a marked stability of  $R_g$  and of the overall protein structure. The average RMSD of the core region (residues 9 to 32) was about 0.2 nm, while for the whole protein was 0.3 nm, consistently with the high core stability already pointed out by Duan and Kollman (see Figure 2) [25]. In accord with this study and more recent ones [34], the dynamical evolution appears to entail a substantial movement of the helix at the N terminal which is responsible for the RMSD increase in the last 7 ns of the trajectory.

For reasons of brevity, of the seven simulations (F1, F2, ... F7) carried out starting from the reconstructed MC conformations we shall typically concentrate on four of them: F1, F3, F4 and F7, which exemplify the variety of observed dynamical behavior.

To summarize and illustrate the system dynamics we report the time evolution of several quantities including the radius of gyration, the RMSD from the native state. Several clues about the dynamical behavior are further obtained by inspecting the evolution of helical content in the protein (measured by means of the DSSP criterion). In this context, when referring to the native helical content, we shall follow the notation of Duan and Kollman and denote with H1, H2 and H3 the regions involving residues 4–8, 15–18 and 23–30, respectively. As a further characterization of the degree of nativeness we have also calculated, at various stages of the simulation, the length of the largest protein segment(s) whose RMSD from the native state is lower than 0.25 nm (see Fig. 3). This cutoff distance was chosen because it represents an upper limit for the structural heterogeneity observed among conformations compatible with the experimental indications. In fact, within this threshold nearly all the NMR models are compatible with each other (while the maximum RMSD deviation between the reference structure of the 1VII PDB entry and any other NMR models is 2.1 Å).

As visible in Fig. 4 the structure evolving in simulation F1, after a short equilibration time, undergoes a rapid compaction as shown by the decrease of  $R_g$  from an initial value of 1.2 nm to about the native one,  $R_g^N \approx 0.89$  nm. The collapse in F1 is not only rapid, but also ordered and productive of tertiary structures yielding a core RMSD of 0.27 nm from the minimized average NMR determined structure (Fig. 4 lower panel). The number of consecutive residues whose RMSD is less than 0.25 nm from the NMR determined structure is stable around 22 residues, that is about 60% of the whole structure (Fig. 3). The helical content corresponding to segments H2 and H3 is well conserved during the simulation time (Fig. 5). The flexibility of the N-terminal region prevents the formation of an optimal helical geometry of the H1 segment. The RMSD value of the whole sequence with respect to the NMR determined structure stabilizes at values around 0.40 nm. The minimum RMSD value calculated over the whole ensemble of 29 model structures respecting the whole set of NMR restraints is as low as 0.23 nm for the core region and 0.35 nm for the whole protein.

The starting structures of the other simulations were substantially more compact than F1 with  $R_g$  values of about 1 nm (see Fig. 6). The selected structures typically display a non-negligible content of secondary structure, as visible in Fig. 5. The inspection of overall native similarity parameters, such as the RMSD, shows that a number of these runs does not exhibit, within the simulated time span, any trend of systematic approach of the native structure or native basin (Fig. 6).

Trajectory F3 displays a particularly interesting behavior. The DSSP analysis reveals that helices H1, H2 and H3 are correctly formed (Fig. 5). However, within the simulated time span the trajectory is not approaching the native conformation since the RMSD from the native state stabilizes around 0.6 nm (Fig. 6, black line). The secondary elements, while formed in the correct native helical regions, assemble in a non-native geometry mainly due to the formation of a stable hydrophobic core involving Phe11, Leu21, Trp24 and Leu29.

A markedly different behavior is recorded in e.g. run F4 where (1) the initial native similarity is acceptable, the core RMSD core being  $\approx 0.45$  nm (Fig. 6), (2) there is a good helical content in H1 and H3 and (3) there are stretches of more than ten consecutive residues below the RMSD threshold of 0.25 nm. This initially promisingly similarity is, however, rapidly lost in a few ns of dynamical evolution, eventually leading to negligible helical content and overall native similarity. Interestingly, the loss of native structure content is paralleled by the formation of a turn conformation involving residues 8–10 and the paring of  $\beta$ -like structures involving residues 2–7 and 10–15.

The tendency of the same segments to form  $\beta$  structures is further observed on trajectories starting from conformations without significant helical content. This effect is here exemplified by run F7 (see Figs. 6-7).

In summary, on the simulated time-scales, all-atom MD runs starting from different selected structures display rather different behaviors depending on the initial degree of compactness and native helical content. In particular, the rapid progress towards the native villin structure was observed in the case where the starting conformation was not too compact and with good helical content in regions H2 and H3. On the other hand, if the initial structure is rather compact and poor in helical content then hydrophobic clusters are likely to form since they lead to a rapid lowering of the protein internal energy. Interestingly, the latter remains higher than the one achieved in F1 or in the protein native state. In fact, the average internal energy of runs F2–F7 is

in the range  $[-1078, -1021]$  KJ/mol while for run F1 and the native structure we observe -1109 and -1094 KJ/mol, respectively. Moreover, the “eager” energy gain brought about by the hydrophobic clusters leads to structures with several non-native long-range contacts (in terms of the sequence separation). This fact implies that a further progress towards the native state requires major structural rearrangements.

Besides the native trajectory, we have considered another reference case constituted by runs started from fully extended conformation of HP36 (Fig. 8). These runs are important to check the possibility to reach states with some degree of nativeness from completely open conformations. In all the cases examined, the extended structures rapidly collapse from the all-extended conformation to compact ones in which no secondary or tertiary structure ordering occurs on the same MD time scales of trajectories F1-F7. These runs were stopped after 20 ns since MD at 300 K is unable to induce the conformational changes necessary to break the compact and disordered globular structures obtained, and because the number of required water molecules made computation extremely slow. In all the simulations, the structures become more compact because of solvent exclusion from the contact with hydrophobic side-chains. This sort of hydrophobic collapse, at least in the time spans analyzed here, is not enough to bring about the ordering of local structures needed to move in the proximity of the native basin.

## Discussion

The present study aims at improving the reach of ordinary MD folding simulations by recouring to a preliminary, simplified, Monte Carlo exploration of the free-energy landscape. If the free-energy landscape associated to the simplified MC dynamics retained all the relevant features of the true one, we could expect that the all-atom MD simulations started from the sampled conformations are expected to have significant advantages over, e.g. those starting from fully extended protein configurations which can be affected by significant lag-phases[35]. The advantage could, however, be more conspicuous if the MC procedure allowed to pick structures from the protein transition state ensemble, in which case the all-atom dynamics would progress towards the native ensemble in a time scale much shorter than the protein typical folding time.

Thus, the expectation is that the two-stage MC-MD trajectories are “time-advanced” with respect to those started, e.g. from extended or other subjectively-chosen conformations. The quantification of the expected time-advancement would be transparent and straightforward if the folding process could be characterized in terms of one (or more) reaction coordinates. All the natural and intuitive order-parameters (such as  $R_g$ , RMSD, buried hydrophobic surface etc.) however appear inadequate to this scope due to their wide degree of fluctuation already observed by Duan and Kollman (and found also in the present study) at all stages of their  $1\mu\text{s}$ -long folding trajectory. Therefore, the benefits of the present strategy can be ascertained only through the comparison of the degree of order and “nativeness” of the explored trajectories compared to that achievable by e.g. starting from extended conformations.

Therefore, we first discuss the reference cases constituted by the runs carried out starting from the native structure and from extended conformations. Over the simulated time scale, the native run appears to be very stable, the only appreciable structural changes involving the mobile regions outside the protein core. We have monitored the stability of the local and non-local native contacts. Two amino acids are said to be in contact if the spatial separation of their  $C_\alpha$ 's is below  $7.5 \text{ \AA}$ . We classify as local contacts those involving residues at a sequence separation equal to three or four (i.e. we omit from the count the non-informative contribution of separation 1 or 2). The native structure possesses 52 distinct local contacts, while the non-local ones, pertaining to sequence separation greater than 5 are 13. In the native run the fraction of local native contacts maintained during the simulation has the nearly constant value of  $q_l = 0.9$ . The non-local one,  $q_{nl}$  instead, due to the mobility of the N-terminus, oscillates between 0.55 and 0.75. The overall RMSD from the native structure remains low and compatible with what found in ref. 25, despite the use of a different force-field.

The high RMSD observed in runs started from the extended structures are obviously reflected in low values for both  $q_l$  and  $q_{nl}$ . In particular,  $q_l$  typically fluctuates between 0.2 and 0.3, while  $q_{nl}$  is practically zero. This does not imply that long-range contacts are absent. On the contrary, as mentioned in the results section, all extended runs evolve rapidly towards globular conformations, and hence with non-local contacts, with formed hydrophobic clusters (different across the runs).

The coarse-grained structures sampled at the collapse temperature,  $T_c$ , have various degree of compactness with  $R_g$  ranging between 8 and  $13 \text{ \AA}$ . As a consequence the sampled conformations have a good degree of structural heterogeneity, since the average RMSD between any pair of these structures is  $5.9 \pm 1.2 \text{ \AA}$ , while the typical RMSD against the core of the villin headpiece is  $7.1 \pm 1 \text{ \AA}$ . Out of these ensemble ten structures were randomly selected; since their mutual RMSD was not inferior to  $6 \text{ \AA}$  they represent well the structural diversity encountered at  $T_c$ . After the reconstruction and energy-minimization procedure these structures were used as inputs for the MD runs. All these starting conformations had a degree of local native similarity substantially higher than what achieved in the extended runs, as summarized in table I. The observed degree of native similarity is not the result of a “blind”, featureless, compactification, but reflects the fact that the coarse-grained model indeed captures some of the physico-chemical forces that govern the folding process. To ascertain this we have applied the same MC scheme on a sequence obtained by a random reshuffling of the villin one. Despite the preservation of the native composition, which must

reflect in an overall bias towards local helical conformations, the native similarity at  $T_c$  in this second situation is appreciably different. In fact, the average values of  $q_l$  and  $q_{nl}$  are 0.25 and 0.08, respectively, while the average RMSD against the protein core is 8.2 Å.

On the contrary,  $q_l$  ranged from 0.3, for F6, to more than 0.6, for cases F1 and F3 which had partially-formed helices in the correct regions. In these two runs, the initially good local similarity is further improved in about 10 ns of evolution, reaching  $q_l \approx 0.8$ . As pointed out in the results section, despite the presence of well-formed helices the tertiary organization found in the two runs is distinctly different. This is reflected by  $q_{nl}$  which starts from a negligible value in both cases and reaches again in about 10 ns of evolution the excellent peak value of 0.75 for F1 (and then stabilizing to 0.7), while it remains virtually zero for the whole F3 run. The case of two trajectories containing structures with high native local content but markedly different non-local one provides an appealing illustration of the role played by the interplay of local and non-local interactions for steering the folding process. In fact, the establishment of the correctly-formed non-local contacts appears to be crucial for providing the necessary stability to maintain both the native secondary and tertiary organization. In fact, after the first 10 ns of dynamical evolution, both  $q_l$  and  $q_{nl}$  settle to the stable values of 0.7 and 0.45, respectively. On the contrary, due to the lack of a native (correct) non-local scaffolding the secondary content in simulation F3 is steadily degraded, dropping from 0.8 to 0.5, in the subsequent evolution. A similar erosion of the native local similarity is further encountered for simulation F4. The starting value of  $q_l \approx 0.5$  which falls to values of about 0.25 due to the lack of a substantial native non-local network of interaction (the typical value of  $q_{nl}$  being about 0.3). The evolution of trajectory F7 is, among all those started from MC-sampled configurations, the one that has the worst performance, since the average value of  $q_l$  is only about 0.3 while  $q_{nl}$  is negligible.

The analysis of several dynamical parameters and the inspection of structures sampled from the MD runs shows that there are several mechanisms responsible for thwarting the dynamics towards states with low native similarity. For trajectory F3, the inability to attain the correct helical packing is due to the formation of a hydrophobic cluster involving Phe11, Leu21, Trp24 and Leu29 which traps the system and prevents its further evolution on the simulated time-scale. The cases of the other trajectories that, on the simulated time scale, do not evolve towards the native basin is somewhat different from the previous one. It appears that a systematic mechanism that opposes and destabilizes the formation or packing of the native helices in the native fold is the tendency to form  $\beta$ -sheets. In fact, concomitant with the disruption of helical content (especially of the “frail” H1 helical region) we have observed the systematic appearance of extended regions (strands) in the protein. This is visible, for example, in Fig. 5 and 7 where the existence of extended conformations as well as their stability under subsequent dynamical evolution is evident. A more precise insight in the mechanism leading to  $\beta$ -sheets is obtained by examining the sequences of the residues taking part into the strands. Both sequence 2–7 and 10–15 contain hydrophobic residues such as Phe7, Phe11, Met 13 and Val10. These residues have unfavorable interactions with water, and one mechanism to minimize the contact is the packing of hydrophobic side-chains in adjacent extended regions of  $\beta$ -structure.

Moreover, the short stretch of the three native helical segments, is such that each individual helix is not expected, on the basis of helix-coil transition models, to be stable on its own but ought to rely on additional mid- and long-range interactions in terms of sequence separation. The importance of optimal mid- and long-range has been recently verified experimentally by Raleigh and coworkers [63]. These authors systematically studied through CD and NMR spectroscopy peptides spanning different regions of HP36, and showed that only when tertiary interactions are present in a sequence comprising at least two helices, a significant amount of ordered structure is present.

In this picture, a generic hydrophobic collapse is thus not enough to determine the onset of a sufficient number of native-like interactions necessary for driving the system in proximity of the native basin. A different kind of structural organization appears to be required, based on the harmonious interplay of non-local interactions with the local ones favoring helical conformations [2]. This picture is consistent with the topomer search mechanism which assumes that the rapid progress towards the native state is possible only after the establishment, in a diffusive conformational search, of a minimal set of contacts embodying the main traits of a protein native topology [64]. In this scheme a paramount role is played by mid-range interactions [2, 64, 65, 66].

The emphasis here is that, for the case of the villin headpiece, the structures leading to this correct interplay of short and long-range contacts can be generated through a preliminary stochastic search of the simplified free-energy landscape. All-atom and explicit-solvent MD runs starting from these configurations present significant advantages over the traditional choice of extended conformations. In fact, the regions in structure-space visited by the seven trajectories considered here are on average much closer to the native basin than for extended runs. Not only there is a benefit in terms of the quality and variety of the trajectories, but there is a further advantage in terms of computational expenditure. In fact, the necessity to take explicitly into account the solvent during the simulation [32], implies that a very large number of water molecules need to be considered in the simulation cell enclosing extended starting simulations. Though this number can be decreased as the protein compactifies, it impacts severely on the total simulation time so that reaching the same-simulation time of e.g. 20 ns each extended run typically requires a sixfold CPU increase over cases F1-F7.

The validity and power of the method discussed here is revealed not only by the typical improvement of the two-stage runs against the extended case, but especially by the ability to reach and maintain the villin HP36 core during simulation F1. This success reflects the viability of both the starting structure picked by the MC search and of the MD force field. In fact, as visible

in Fig. 4 the F1 starting structure is not similar to the native state but it presents the possibility of rapidly evolving towards it due to the presence of two partial native helices in an overall non-compact conformation. It is the action of the force-field that makes this progression possible (of course after the reconstruction of the atom detail from the coarse model).

The representative structure of run F1 (determined through the application of the structural clustering method described by Daura and coworkers [67]) has an RMSD over the core region of 0.27 nm from the minimized average NMR structure, and a minimum of only 0.24 nm over the whole set of 29 NMR models. This represents an improvement over the landmark result of Duan and Kollman [25] who obtained an RMSD of 0.4 nm with a threefold increase of simulation time. The significance of the degree of nativeness obtained here for the HP36 core is highlighted by two facts. First, the core RMSD is smaller than typical thresholds used to define a successfully-folded conformation in similar contexts (and for analogous lengths)[68]. Secondly, it should be borne in mind that the 29 NMR models of the Villin headpiece have a non-negligible degree of structural heterogeneity among themselves (up to nearly 3 Å), with the maximum RMSD difference between the minimized average NMR structure (PDB code 1vii) and any other model being 0.21 nm.

To summarize, we have followed the all-atom dynamical evolution of the Villin headpiece starting from several configurations obtained by a coarse exploration of the system energy landscape. The seven simulated trajectories included a notable instance where a correctly-folded configuration of the protein core was reached and maintained. Furthermore, the significant secondary content and organization found in all starting structures resulted in interesting dynamical evolutions that, even when not progressing towards the folded state, convey valuable information on the folding process, as the trapping mechanism associated with the formation of contacting strands. The protocol used here has been kept as general and unbiased as possible and may be further extended e.g. at the level of the coarse-grained model and/or of the selection criteria of the starting structures. Therefore, the proposed strategy ought to be applicable to other instances of short proteins with significant advantages over the use of extended structures as the default unbiased starting point of all-atom dynamical simulations with explicit solvent.

## Materials and methods

### Molecular Dynamics simulations and analysis

Every all-atom Molecular Dynamics Experiment was run using the same simulation protocol and conditions. In the simulations starting from the NMR, completely extended and reconstructed conformations derived from the preliminary MC analysis (runs F1 to F7), all basic  $\text{NH}_2$  groups were considered protonated while all the acidic  $\text{COO}^-$  groups were considered deprotonated. These conditions resulted in a total charge of +2 on the protein. The protein in each simulation was solvated with explicit water molecules in a period octahedral box large enough to contain the protein and 1.0 nm of solvent on all sides. The simple point charge (SPC) [69] water model was used to simulate the solvent. Electroneutrality of the system was ensured by the addition of two negatively charged chloride ions. Table I reports the number of water molecules in each simulation. The same equilibration protocol was used in all simulation:

1. Each system was initially energy minimized with a steepest descent method for 1000 steps. The calculation of electrostatic forces utilized the PME implementation of the Ewald summation method [70]. The GROMOS96 force field [71, 72] was used.
2. To release excess strain in simulations F1–F7 due to possible artifacts in the reconstruction procedure, three sequential MD runs of 50 ps each with position restraints on the protein, backbone and sidechains, respectively. In the first, the protein atoms were kept fixed with the solvent molecules free to move. In the subsequent run, the backbone of the protein was kept fixed with both the sidechains and solvent free to move in MD. In the third and final simulation, the sidechains were kept fixed, while the backbone and solvent atoms were allowed to move.
3. After these first relaxation steps, each system was heated to 300K by 200 ps of MD simulation under NPT conditions, with no restraints, by weak coupling to a bath of constant pressure ( $P_0 = 1$  bar, coupling time  $\tau_P = 0.5$  ps) [73].
4. Each of the systems was then equilibrated by 50 ps of unrestrained MD with coupling to an external temperature bath [73] with coupling constant of 0.1 ps.
5. The production runs at 300K, using NPT conditions were 50 ns long in the case of the simulation starting from the NMR determined structure 1VII.pdb and simulations F1 to F7. Due to the extremely high number of explicit water molecules, the three independent MD simulations starting from the totally extended conformation were run for 20 ns. In all production runs, the temperature was maintained close to the intended values, by weak coupling to an external temperature bath [73] with a coupling constant of 0.1 ps. The protein and the rest of the system were coupled separately to the temperature bath.

The LINCS algorithm [74] was used to constrain all bond lengths. For the water molecules the SETTLE algorithm [75] was used. A dielectric permittivity,  $\epsilon = 1$ , and a time step of 2 fs were used. All atoms were given an initial velocity obtained from a Maxwellian distribution at the desired initial temperature of 300K.

The extended conformation of the protein was generated with Swiss-PdBViewer [76] and the system was solvated with the same protocol used for the folding simulations.

All the minimization, MD runs and analysis of the trajectories were performed using the GROMACS software package. [77] The graphical representations of the protein were realized with the program MOLMOL [78].

Simulation	Water Molecules	$q_l^0$	$q_{nl}^0$	initial core RMSD
F1	6568	0.67	0.1	8.4
F2	5187	0.50	0.05	8.5
F3	3892	0.61	0.15	6.1
F4	3140	0.50	0.10	4.5
F5	2466	0.42	0.23	4.8
F6	2848	0.31	0.11	7.0
F7	2911	0.46	0.04	5.5
E1	11661			
E2	8560			
E3	7272			
Native	2768			

TABLE I: Summary of the main feature of the various MD runs Number of solvent particles in each of the simulations. For trajectories F1-F7 are also provided the fraction of local and non-local native contacts at the beginning of the MD run, as well as the initial RMSD over the core of the protein (residues 9-32).

### Monte Carlo

The starting configurations for all-atom MD simulation were obtained from a preliminary Monte Carlo exploration of the configurational space. In order to make this preliminary search as efficient as possible we have adopted a simplified representation of protein conformations. Most of the procedures adopted to coarse grain the microscopic degrees of freedom of proteins substitute a whole amino acid with a small number of effective centroids. We have followed this choice and used effective  $C_\alpha$  and  $C_\beta$  centroids for each amino acid (with the exception of Gly which lacks the  $C_\beta$  centroid). This choice brings about a drastic simplification for the structure of the Hamiltonian which will involve only interactions between the centroids. In particular we regard the  $C_\alpha$  centroids as the centers of the effective interactions among contacting residues. The  $C_\beta$  ones play, instead, a passive role being used to capture the steric hindrance of the sidechains. In order to minimize the dimensionality of conformational space only the  $C_\alpha$  degrees of freedom were considered and the effective  $C_\beta$ 's were constructed according to the Park and Levitt rule [79].

The dynamics in conformation space is carried out using a Monte Carlo technique. At each attempted Monte Carlo step the current conformation ( $C_\alpha$ -trace) is distorted by means of crankshaft and pivot rotations. These types of moves are employed since they do not alter the separation of consecutive  $C_\alpha$ 's (bond length). The newly generated conformation is then accepted/rejected according to the standard Metropolis rule. The system energy function comprises the following terms:

$$\mathcal{H} = \mathcal{H}_{steric} + \mathcal{H}_{pairwise} + \mathcal{H}_{cooperative} + \mathcal{H}_{chiral} . \quad (1)$$

The first term,  $\mathcal{H}_{steric}$ , is used to enforce some basic steric constraints on the conformations generated with the MC procedure. These knowledge-based constraints involve both two- and three-body terms. In particular, no two centroids of distinct residues,  $i$  and  $j$  (be they  $C_\alpha$  or  $C_\beta$ ) are allowed to come at a distance smaller than 3.0 Å, with the proviso that if  $|i - j| = 2$  then their minimal separation is set to 5 Å. These pairwise constraints need to be complemented by suitable three-body terms for a more accurate treatment of steric hindrance. In fact, it has been shown that proteins are well-described as “tubes” with a uniform effective thickness of about  $\Delta = 2.7$  Å [80, 81]. This implies that the local radius of curvature of the backbone (the  $C_\alpha$  trace) cannot be smaller than  $\Delta$  and that two distinct backbone portions cannot come at a separation smaller than  $2\Delta$ . From

a numerical point of view these requirements are enforced by ensuring that the radius of the circumference going through any triplet of distinct  $C_\alpha$ 's is greater than  $\Delta$ .

The second energy term,  $\mathcal{H}_{pairwise}$  is used, instead, to capture the effective interactions among pairs of sufficiently closed residues. The strength of the contact interaction between two residues  $i$  and  $j$  is modulated with a sigmoidal function,  $f(r_{i,j})$ , which depends on the separation of the corresponding  $C_\alpha$  centroids,  $r_{i,j}$ , and has a point of inflection at 6.5 Å,

$$f(r_{i,j}) = \frac{1}{2} + \frac{1}{2} \tanh(6.5 - r_{i,j}) \quad (2)$$

Therefore,  $\mathcal{H}_{pairwise}$  can be written as

$$\mathcal{H}_{pairwise} = \sum_{i,j}^l \epsilon(S_i, S_j) f(r_{ij}) \quad (3)$$

where the prime denotes that the summation runs over non-consecutive residues,  $S_i$  denotes the type of residue at the sequence position  $i$  and  $\epsilon$  is the symmetric matrix describing the strength of the effective residue-residue interactions. Various criteria have been employed to extract tables of effective potentials. Here we resorted to the one developed by Kolinsky, Godzik and Skolnick [82] which proved useful to identify the correct fold of short proteins [83]. In addition, in analogy with ref. 83, we have introduced a cooperative four-body interaction meant to favor the packing of secondary motifs:

$$\mathcal{H}_{cooperative} = \sum_{i,j,a,b} f(r_{i,j}) f(r_{i+a,j+b}) [\epsilon(S_i, S_j) + \epsilon(S_{i+a}, S_{j+b})] / 20 \quad (4)$$

where  $a$  and  $b$  can take on the values  $\{\pm 3, \pm 4\}$ . This term introduces an additional energy contribution if both bonds  $(i, j)$  and  $(i + a, j + b)$  are present.

Besides these interactions we have further found useful to reduce the structural freedom of the coarse-grained conformations by introducing a knowledge-based chiral potential,  $\mathcal{H}_{chiral}$ . The chiral bias and constraints were derived by parsing several structurally independent proteins into fragments of 4 consecutive residues. For each fragment we computed the end-to-end distance,  $r$ , and the associated chirality  $\chi = (\vec{b}_{12} \times \vec{b}_{23}) \cdot \vec{b}_{34}$  where  $\vec{b}_{ij}$  denotes the normalized vector joining the  $i$ th and  $j$ th  $C_\alpha$  centroids in the fragment. The scatter plot  $\chi$  vs  $r$  of Fig. 9 shows that some regions (in principle compatible with feasible configurations) are forbidden, or very rarely populated. This fact is used to preclude these regions from being explored by the MC dynamics. More precisely, any fragment  $(i, i + 4)$  of any configuration encountered in the stochastic dynamics has to avoid the following regions of the  $\chi, r$  plane (the constraints are enforced again through a large energy penalty): (a)  $\chi < 0$  and  $r < 7.5\text{Å}$ , (b)  $r > 11\text{Å}$ , (c)  $r < 4\text{Å}$ . It is also possible to notice that a large number of configurations cluster around the point  $(\chi \approx 0.7, r \approx 5.5\text{Å})$  which corresponds to helical conformations; the other highly populated band corresponding to  $r > 9\text{Å}$  is instead associated with extended conformations.

In the absence of any chiral bias, besides the constraints mentioned above the MC sampling tends not to occupy the helical region even for sequences with strong helical propensities. We therefore introduced a sequence-dependent bias to favor the occupation of the helical region in such cases. This is accomplished by processing the set of proteins representatives (obtained from the PDBselect list [84, 85]) to calculate the probability of each amino acid to be in fragments having helical (H) or extended (E) conformations in the various protein instances. The calculated values are given in Table II (notice that since each amino acid can occupy other portions of the phase diagram,  $p_H$  and  $p_E$  do not sum to 1). Within the MC scheme, this knowledge-based information is exploited by calculating, for each fragment of four consecutive residues, the value of helical and extended probability,  $\bar{p}_H$  and  $\bar{p}_E$ , averaged over the four residues. The occupation of the helical region of the  $\chi - r$  plane is favored if  $\bar{p}_H$  is sufficiently high and, concomitantly,  $\bar{p}_E$  is sufficiently low.

A test on an independent set of proteins has shown that a useful criterion to identify putative helical fragments is to require that  $p_H(1 - p_E) > 0.25$  and  $p_E(1 - p_H) < 0.15$ . These inequalities ensure that about 50 % of helical fragments are correctly recognized, while the probability that an extended fragment is mistakenly labeled as helical is about 10%. Each putative helical fragment is biased towards occupying the helical region of the  $\chi, r$  plane through the following potential term:

$$V(\chi, r) = \frac{1}{2} + \frac{1}{2} \tanh\left[\frac{\chi - 0.7}{\sigma_\chi}\right] \tanh\left[\frac{5.5 - r}{\sigma_r}\right]. \quad (5)$$

The values of  $\sigma_\chi$  and  $\sigma_r$  are set to 0.1 and 0.3, respectively to reflect the spread observed in the  $\chi - r$  distribution of helical fragments. These potential biases are accumulated in the energy term  $\mathcal{H}_{chiral}$ :



a.a.	$p_H$	$p_E$	a.a.	$p_H$	$p_E$
ALA	0.45	0.19	LEU	0.40	0.24
ARG	0.38	0.21	LYS	0.35	0.20
ASN	0.28	0.18	MET	0.42	0.24
ASP	0.32	0.17	PHE	0.31	0.32
CYS	0.27	0.23	PRO	0.16	0.19
GLN	0.43	0.19	SER	0.30	0.22
GLU	0.43	0.18	THR	0.28	0.27
GLY	0.18	0.21	TRP	0.31	0.28
HIS	0.27	0.25	TYR	0.28	0.32
ILE	0.32	0.34	VAL	0.26	0.39

TABLE II: Probability of the different amino acids to be in helical or extended conformations. The probabilities, indicated with  $p_H$  and  $p_E$ , were calculated by processing a set of nearly 140 structures determined by high-resolution Xray crystallography and reported in the PDBselect list of protein representatives.

$$\mathcal{H}_{chiral} = V_0 \sum_l V(\chi_l, r_l) \quad (6)$$

where the sum runs over all putative helical fragments of four residues and the amplitude coefficient,  $V_0$ , is equal to 3.0. This value was chosen after applying the MC sampling strategy to various short proteins (from about 30 to 50 residues) belonging to different structural families, (PDB codes 1aie, 1ajj, 1ppt, 1ptq, 2erl). We stress again that, in our scheme, we have not found the necessity to add any bias towards extended conformations for local sequences that were not putatively helical. Indeed, for  $\beta$  proteins of length comparable to the villin headpiece (e.g. 1eit, 1pmc) virtually no residues can be found in helical conformations at all MC temperatures. Finally, the MC exploration was performed starting from extended conformations at high  $T$  and then gradually lowering the temperature as in traditional simulated annealing schemes. For  $V_0 \approx 3.0$  the formation of secondary structures occurred at about the collapse temperature (i.e. the temperature where a rapid decrease of the radius of gyration occurs). In this situation, the presence of secondary structures results from a physically-appealing similar interplay of the sequence-dependent chiral bias and of the more complicated energy terms.

In essence, the present Hamiltonian embodies the main ingredients that are regarded as crucial in coarse-grained approaches to protein folding, namely pairwise interactions, local biases for backbone chirality and cooperative interactions to promote the packing of secondary motifs. Therefore, the interesting and rich MD evolution of the reconstructed coarse-grained structures is indicative that the two-stage scheme can be profitably used under quite general conditions, and not the necessity to use the present coarse-grained energy functional. In particular a foreseeable improvement to the present Hamiltonian would be to substitute the cooperative term by a suitable modeling of main-chain hydrogen bonds. This has, in fact, proved to be an important ingredient to aid the formation of beta-sheets structures in globular proteins [86].

### Reconstruction procedure

As explained above, all the protein conformations generated through the Monte Carlo procedure have a simplified structural representation essentially described by the  $C_\alpha$  degrees of freedom. These coarse-grained structures need to be reconstructed with all the atomic detail before they can be processed in ordinary all-atom molecular dynamics schemes.

The problem of reconstructing reliably a protein's atomic detail starting from a coarse-grained representation has been addressed previously. Several studies have appeared which address the problem of reconstructing, with full atomic detail, a protein's backbone and/or sidechains starting from very limited structural informations [87, 88, 89, 90, 91]. In the present study we have developed a novel knowledge-based strategy that is simple and whose accuracy is not inferior to more sophisticated techniques. We now illustrate this reconstruction scheme. For reasons of space our description will be complete, but schematic; a more detailed presentation of the method and its performance will be published in the future.

The algorithm that reconstructs the full atomic detail of a given  $C_\alpha$  trace is based on the use of a library of protein fragments built from about 100 NMR gapless structures taken from the PDBselect list[84, 85]. These structures were parsed into template fragments of four consecutive residues retaining the whole atomic detail of the mainchain and of the sidechains of the middle

residues. For each set of four consecutive  $C_\alpha$ 's in the  $C_\alpha$  trace one finds the best superimposable fragment in the library and assigns the central peptide plane to the protein to be reconstructed after an optimal roto-translation [92]; the first and last peptide planes are treated separately. Finally, the sidechain of any given residue,  $R$ , is obtained by first considering only the set of template fragments where one of the middle residues,  $R'$ , is of the same type as  $R$ . Next, after aligning (in sequence)  $R$  and  $R'$ , the sidechain of  $R$  is assigned (again after an optimal roto-translation) from the fragment providing the best superposition with the reconstructed backbone.

In Fig. 10 we have reported the distribution for the errors in the reconstruction of known protein structures. It appears that 70 % of the heavy atoms are placed within 1 Å of the crystallographic positions (and 62 % within only 0.5 Å). Although the typical performance is very satisfactory, it is worth pointing out that, as for other methods, a wrong placement of ramified sidechains can occasionally give rise to large deviations from the correct positions (see the tail of the error distribution in Fig. 10). Large deviations may also be encountered in correspondence of charged residues, whose sidechain orientation is heavily influenced by the local electrostatic (obviously not captured in our simple reconstruction scheme). This is, however, a minor problem in this context, since the reconstructed structure is solvated, energy-minimized and equilibrated before starting the MD run.

**Acknowledgments.** We acknowledge support from CNR, INFN and MIUR Cofin 2003.

- 
- [1] Anfinsen, C. B. Principles that govern the folding of protein chains. *Science* 181:223–230, 1973.
  - [2] Anfinsen, C. and Scheraga, H. Experimental and theoretical aspects of protein folding. *Adv. Protein Chem.* 29:205–299, 1975.
  - [3] Branden, C. and Tooze, J. Introduction to protein structure. Garland Publishing, New York, , 1991.
  - [4] Creighton, T. Proteins, structure and molecular properties. W.H. Freeman and Company, New York, second edition, , 1993.
  - [5] Fersht, A. R. Structure and Mechanism in Protein Science. V. H. Freeman and Co., New York, , 1999.
  - [6] Bryngelson, J. D., Onuchic, J. N., Socci, N. D., and Wolynes, P. G. Funnels and pathways and the energy landscape of protein folding: A synthesis. *Proteins* 21:167–195, 1995.
  - [7] Wolynes, P. G., Onuchic, J. N., and Thirumalai, D. Navigating the folding routes. *Science* 267:1619–1620, 1995.
  - [8] Dill, K. A. and Chan, H. S. From Levinthal to pathways to funnels. *Nature Structural Biology* 4:10–19, 1997.
  - [9] Dobson, C., Sali, A., and Karplus, M. Protein folding: A perspective from theory and experiment. *Angew. Chem. Int. Edit.* 37:868–893, 1998.
  - [10] Sali, A., Shakhnovich, E., and Karplus, M. How does a protein fold. *Nature* 369:248–251, 1994.
  - [11] Levinthal, C. Mossbauer Spectroscopy in Biological Systems. Univ. Illinois Press, , 1969.
  - [12] Micheletti, C., Banavar, J. R., Maritan, A., and Seno, F. Protein structures and optimal folding from a geometrical variational principle. *Phys. Rev. Lett.* 82:3372–3375, 1999.
  - [13] Mirny, L. A., Abkevich, V. I., and Shakhnovich, E. I. How evolution makes proteins fold quickly. *Proc. Natl. Acad. Sci., USA* 95:4976–4981, 1998.
  - [14] Venclovas, C., Zemla, A., Fidelis, K., and Moulton, J. Comparison of performance in successive casp experiments. *Proteins: Structure Function and Genetics* 45:163–170, 2001.
  - [15] Venclovas, C. Comparative modeling in casp5: Progress is evident, but alignment errors remain a significant hindrance. *Proteins: Structure Function and Genetics* 53:380–388, 2003.
  - [16] Venclovas, C., Zemla, A., Fidelis, K., and Moulton, J. Assessment of progress over the casp experiments. *Proteins: Structure Function and Genetics* 53:585–595, 2003.
  - [17] Vila, J., Ripoll, D., and Scheraga, H. A. Atomically detailed folding simulation of the b domain of staphylococcal protein a from random structures. *Proc. Natl. Acad. Sci. USA* 100:14812–14816, 2003.
  - [18] Berendsen, H. A glimpse of the holy grail? *Science* 282:642–643, 1998.
  - [19] Brooks, C. Simulations of protein folding and unfolding. *Curr. Opin. Struct. Biol.* 8:222–226, 1998.
  - [20] Dobson, C. M., Sali, A., and Karplus, M. Protein folding: A perspective from theory and experiment. *Angew. Chem. Int. Ed.* 37:869–893, 1998.
  - [21] Karplus, M. and McCammon, J. A. Molecular dynamics simulations of biomolecules. *Nat. Struct. Biol.* 9:646–652, 2002.
  - [22] McKnight, C. J., Matsudaira, P. T., and Kim, P. S. Nmr structure of the 35-residue villin headpiece subdomain. *Nat. Struct. Biol.* 4:180–184, 1997.
  - [23] Kubelka, J., Eaton, W., and Hofrichter, J. Experimental tests of villin subdomain folding simulations. *J. Mol. Biol.* 329:625–630, 2003.
  - [24] Wang, M., Y. Tang, S. Sato, Vugmeyster, L., McKnight, C., and Raleigh, D. Dynamic nmr line-shape analysis demonstrates that the villin headpiece subdomain folds on the microsecond time scale. *J. Am. Chem. Soc.* 125:6032–6033, 2003.
  - [25] Duan, Y. and Kollman, P. A. Pathways to a protein folding intermediate observed in a 1-microsecond simulation in aqueous solution. *Science* 282:740–749, 1998.
  - [26] Lee, M. R., Tsai, J., Baker, D., and Kollman, P. A. Molecular dynamics in the endgame of protein structure prediction. *J. Mol. Biol.* 313:417–430, 2001.
  - [27] van der Spoel, D. and Lindahl, E. Brute-force molecular dynamics simulations of villin headpiece: Comparison with nmr parameters. *J. Phys. Chem.* 107:11178–11187, 2003.
  - [28] Lee, M. R., Baker, D., and Kollman, P. A. 2.1 and 1.8 Å average ca rmsd structure predictions on two small proteins, hp-36 and s15. *J. Am. Chem. Soc.* 123:1040–1046, 2001.

- [29] Lin, C., Hu, C., and Hansmann, U. H. E. Parallel tempering simulations of hp-36. *Proteins: Structure, Function, and Genetics* 52:436–445, 2003.
- [30] Shen, M. Y. and Freed, K. F. All-atom fast protein folding simulations: The villin headpiece. *Proteins: Structure, Function and Genetics* 49:439–445, 2002.
- [31] Ripoll, D. R., Vila, J. A., and Scheraga, H. A. Folding of the villin headpiece subdomain from random structures. analysis of the charge distribution as a function of ph. *J. Mol. Biol.* 339:915–925, 2004.
- [32] Papoian, G., Ulander, J., Eastwood, M., Schulten, Z. L., and Wolynes, P. G. Water in protein structure prediction. *Proc. Natl. Acad. Sci. USA* 101:3352–3357, 2004.
- [33] Ferrara, P. and Caffisch, A. Native topology or specific interactions: What is more important for protein folding? *J. Mol. Biol.* 306:837–850, 2001.
- [34] Shirts, M. and Pande, V. S. COMPUTING: Screen Savers of the World Unite! *Science* 290(5498):1903–1904, 2000.
- [35] Fersht, A. R. On the simulation of protein folding by short time scale molecular dynamics and distributed computing. *PNAS* 99(22):14122–14125, 2002.
- [36] Paci, E., Cavalli, A., Vendruscolo, M., and Caffisch, A. Analysis of the distributed computing approach applied to the folding of a small beta peptide. *Proc. Natl. Acad. Sci. USA* 100(14):8217–8222, 2003.
- [37] Unger, R. and Moulton, J. Genetic algorithm for protein folding simulation. *J. Mol. Biol.* 231:75–81, 1993.
- [38] Tesi, M., van Rensburg, E. J., Orlandini, E., and Whittington, S. Monte-carlo study of the interacting self-avoiding walk in three dimension. *J. Stat. Phys.* 82:155–181, 1996.
- [39] Lee, J., Scheraga, H., and Rackovsky, S. New optimization method for conformational energy calculations on polypeptides: Conformational space annealing. *J. Comput. Chem* 18:1222–1232, 1997.
- [40] Irbäck, A. and Potthast, F. Studies of an off-lattice model for protein folding: Sequence dependence and improved sampling at finite temperature. *J. Chem. Phys.* 103:10298–10305, 1995.
- [41] Hansmann, U. and Okamoto, Y. New monte carlo algorithms for protein folding. *Curr. Op. Struct. Biol.* 9:177–183, 1999.
- [42] Scheraga, H. and Hao, M. Entropy sampling monte carlo for polypeptides and proteins. *Adv. Chem. Phys.* 105:243–272, 1999.
- [43] H. Arkin, F. Y., Celik, T., Berg, B., and Meirovitch, H. Multicanonical simulations of some peptides. *Comp. Phys. Comm.* 147:600–603, 2002.
- [44] Garcia, A. and Onuchic, J. Folding a protein in a computer: An atomic description of the folding/unfolding of protein a. *Proc. Natl. Acad. Sci. USA* 100:13898–13903, 2003.
- [45] Baker, D. A. Surprising simplicity to protein folding. *Nature* 405:39–42, 2000.
- [46] Clementi, C., Nymeyer, H., and Onuchic, J. N. Topological and energetic factors: What determines the structural details of the transition state ensemble and 'en-route' intermediates for protein folding? an investigation for small globular proteins. *J. Mol. Biol.* 298:937–953, 2000.
- [47] Klimov, D. K. and Thirumalai, D. Native topology determines force-induced unfolding pathways in globular proteins. *Proc. Natl. Acad. Sci. USA* 97:7254–7259, 2000.
- [48] Hoang, T. X. and Cieplak, M. Sequencing of folding events in go-type proteins. *J. Chem. Phys.* 113:8319–8328, 2000.
- [49] Hao, M. H. and Scheraga, H. A. On foldable protein-like models; a statistical-mechanical study with monte carlo simulations. *Physica A* 244:124–145, 1997.
- [50] Kolinsky, A. and Skolnick, J. Monte carlo simulations of protein folding ii. application to protein a, rop and crambin. *Proteins: Structure Function and Genetics* 18:353–366, 1994.
- [51] Tiana, G. and Broglia, R. A. Statistical analysis of native contact formation in the folding of designed model proteins. *J. Chem. Phys* 114:2503, 2001.
- [52] Lazaridis, T. and Karplus, M. “new view” of protein folding reconciled with the old through multiple unfolding simulations. *Science* 278:1928–1931, 1997.
- [53] Bahar, I., Erman, B., Jernigan, R. L., Atilgan, A. R., and Covell, D. G. Collective motions in hiv-1 reverse transcriptase: Examination of flexibility and enzyme function. *J. Mol. Biol.* 285:1023–1037, 1999.
- [54] Cieplak, M. and Hoang, T. X. Scaling of folding properties in go models of proteins. *J. Biol. Phys.* 26:273–294, 2000.
- [55] Hoang, T. X. and Cieplak, M. Molecular dynamics of folding of secondary structures in go-type models of proteins. *J. Chem. Phys.* 112:6851–6862, 2000.
- [56] Favrin, G., Irbäck, A., and Wallin, S. Folding of a small helical protein using hydrogen bonds and hydrophobicity forces. *Proteins: Structure Function and Genetics* 47:99–105, 2002.
- [57] Vieth, M., Kolinski, A., Brooks, C., and Skolnick, J. Prediction of the folding pathways and structure of the gc4 leucine zipper. *J. Mol. Biol.* 237:361–367, 1994.
- [58] Liwo, A., Pincus, M., Wawak, R., Rackowsky, S., and Scheraga, H. Prediction of protein conformation on the basis of a search for compact structures; test on avian pancreatic polypeptide. *Prot. Sci.* 2:1715–1731, 1993.
- [59] Kaya, H. and Chan, H. S. Energetic components of cooperative protein folding. *Phys. Rev. Lett.* 85:4823–4826, 2000.
- [60] Kaya, H. and Chan, H. S. Polymer principles of protein calorimetric two-state cooperativity. *Proteins: Structure Function and Genetics* 43:523, 2001.
- [61] Hao, M.-H. and Scheraga, H. A. Molecular mechanisms for cooperative folding of proteins. *J. Mol. Biol.* 277:973–983, 1998.
- [62] Shakhnovich, E. and Gutin, A. Engineering of stable and fast-folding sequences of model proteins. *Proc. Natl. Acad. Sci. USA* 90:7195–7199, 1993.
- [63] Tang, Y., Rigotti, D. J., Fairman, R., and Raleigh, D. P. Peptide models provide evidence for significant structure in the denatured state of a rapidly folding protein: the villin headpiece subdomain. *Biochemistry* 43:3264–3272, 2004.
- [64] Debe, D., Carlson, M., and Goddard, W. The topomer-sampling model of protein folding. *Proc. Natl. Acad. Sci. USA* 96:2596–2601, 1999.

- [65] Makarov, D. E. and Plaxco, K. W. The topomer search model: a simple, quantitative theory of two-state protein folding kinetics. *Prot. Sci.* 12:17–26, 2003.
- [66] Shortle, D. and Ackerman, M. S. Persistence of native-like topology in a denatured protein in 8m urea. *Science* 293:487–489, 2001.
- [67] Daura, X., Gademann, K., Jaun, B., Seebach, D., van Gunsteren, W. F., and Mark, A. E. Peptide folding: when simulation meets experiment. *Angew. Chemie Intl. Ed.* 38:236–240, 1999.
- [68] Snow, C. D., Nguyen, H., Pande, V. S., and Gruebele, M. Absolute comparison of simulated and experimental protein-folding dynamics. *Nature* 420:33–34, 2002.
- [69] Berendsen, H. J. C., Grigera, J. R., and Straatsma, T. P. The missing term in effective pair potentials. *J. Phys. Chem.* 91:6269–6271, 1987.
- [70] Darden, T., York, D., and Pedersen, L. Particle mesh ewald. an  $n \cdot \log(n)$  method for ewald sums in large systems. *Journal of Chemical Physics* 98:10089–10092, 1993.
- [71] van Gunsteren, W. F., Daura, X., and Mark, A. E. GROMOS force field. *Encyclopedia of Computational Chemistry* 2:1211–1216, 1998.
- [72] van Gunsteren, W. F., Billeter, S. R., Eising, A. A., Hünenberger, P. H., Krüger, P., Mark, A. E., Scott, W. R. P., and Tironi, I. G. *Biomolecular Simulation: The GROMOS96 Manual and User Guide*. vdf Hochschulverlag, ETH Zürich, Switzerland, , 1996.
- [73] Berendsen, H. J. C., Postma, J. P. M., van Gunsteren, W. F., Di Nola, A., and Haak, J. R. Molecular dynamics with coupling to an external bath. *J. Chem. Phys.* 81:3684, 1984.
- [74] Hess, B., Bekker, H., Fraaije, J. G. E. M., and Berendsen, H. J. C. A linear constraint solver for molecular simulations. *J.Comp.Chem.* 18:1463–1472, 1997.
- [75] Miyamoto, S. and Kollman, P. A. Settle: An analytical version of the shake and rattle algorithms for rigid water models. *J. Comp. Chem.* 13:952–962, 1992.
- [76] Guex, N. and Peitsch, M. C. Swiss-model and the swiss-pdbviewer: An environment for comparative protein modeling. *Electrophoresis* 18:2714–2723, 1997.
- [77] van der Spoel, D., van Drunen, R., and Berendsen, H. J. C. GRoningen MACHine for Chemical Simulations. Department of Biophysical Chemistry, BIOSON Research Institute, Nijenborgh 4 NL-9717 AG Groningen, , 1994. e-mail to gromacs@chem.rug.nl.
- [78] Koradi, R., Billeter, M., and Wuthrich, K. Molmol: A program for display and analysis of macromolecular structures. *J.Mol.Graphics.* 14:51–55, 1996.
- [79] Park, B. and Levitt, M. Energy functions that discriminate x-ray and near-native folds from well-constructed decoys. *Proteins: Structure Function and Genetics* 258:367–392, 1996.
- [80] Maritan, A., Micheletti, C., Trovato, A., and Banavar, J. R. Optimal shapes of compact strings. *Nature* 406:287, 2000.
- [81] Banavar, J., Maritan, A., Micheletti, C., and Trovato, A. Geometry and physics of proteins. *Proteins: Structure Function and Genetics* 47:315–322, 2002.
- [82] Kolinsky, A., Godzik, A., and Skolnick, J. A general method for the prediction of the three dimensional structure and folding pathway of globular proteins: Application to designed helical proteins. *J. Chem. Phys.* 98:7420–7433, 1993.
- [83] Kolinsky, A. and Skolnick, J. Monte carlo simulations of protein folding i. lattice model and interaction scheme. *Proteins: Structure Function and Genetics* 18:338–352, 1994.
- [84] Hobohm, U., Scharf, M., Schneider, R., and Sander, C. Selection of a representative set of structures from the brookhaven protein data bank. *Prot. Sci.* 1:409–417, 1992.
- [85] Hobohm, U. and Sander, C. Enlarged representative set of protein structures. *Prot. Sci.* 2:522, 1992.
- [86] Kolinski, A. and Skolnick, J. Reduced models of proteins and their applications. *Polymer* 45:511–524, 2004.
- [87] Correa, P. The building of protein structures from  $\alpha$ -carbon coordinates. *Proteins: Structure Function and Genetics* 7:366–377, 1990.
- [88] Rey, A. and Skolnick, J. Efficient algorithm for the reconstruction of a protein backbone from the  $\alpha$ -carbon coordinates. *J. Comput. Chem.* 13:443–456, 1991.
- [89] Holm, L. and Sander, C. Database algorithm for generating protein backbone and side-chain co-ordinates from a  $c_\alpha$  trace. application to model building and detection of co-ordinate errors. *J. Mol. Biol.* 218:183–194, 1991.
- [90] Bower, M., Cohen, F., and Dunbrak, R. Prediction of protein side-chain rotamers from a backbone-dependent rotamer library. *J. Mol. Biol.* 267:1268–1282, 1997.
- [91] Kazmierkiewicz, R., Liwo, A., and Scheraga, H. Addition of side chains to a known backbone with defined side-chain centroids. *Biophys. Chem.* 100:261–280, 2003.
- [92] Kabsch, W. A discussion of the solution for the best rotation to relate two sets of vectors. *Acta Crystallogr.* A34:828–829, 1978.

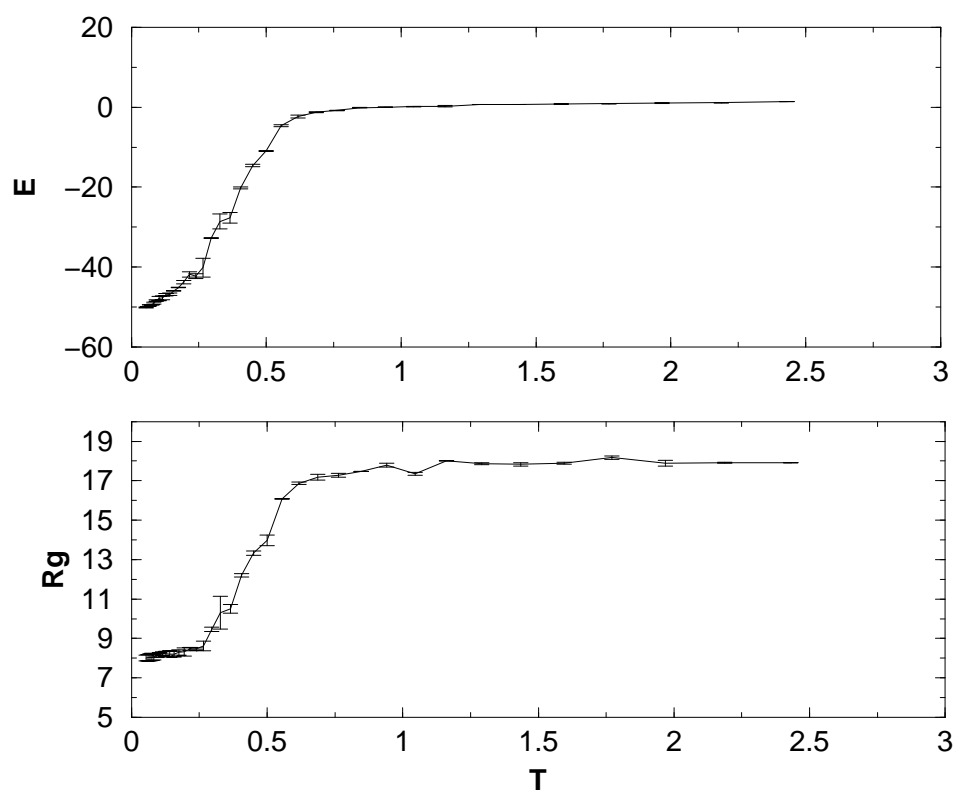


FIG. 1: Average energy and radius of gyration as a function of temperature for the coarse-grained model. For each temperature the averages were calculated over 1000 uncorrelated structures.

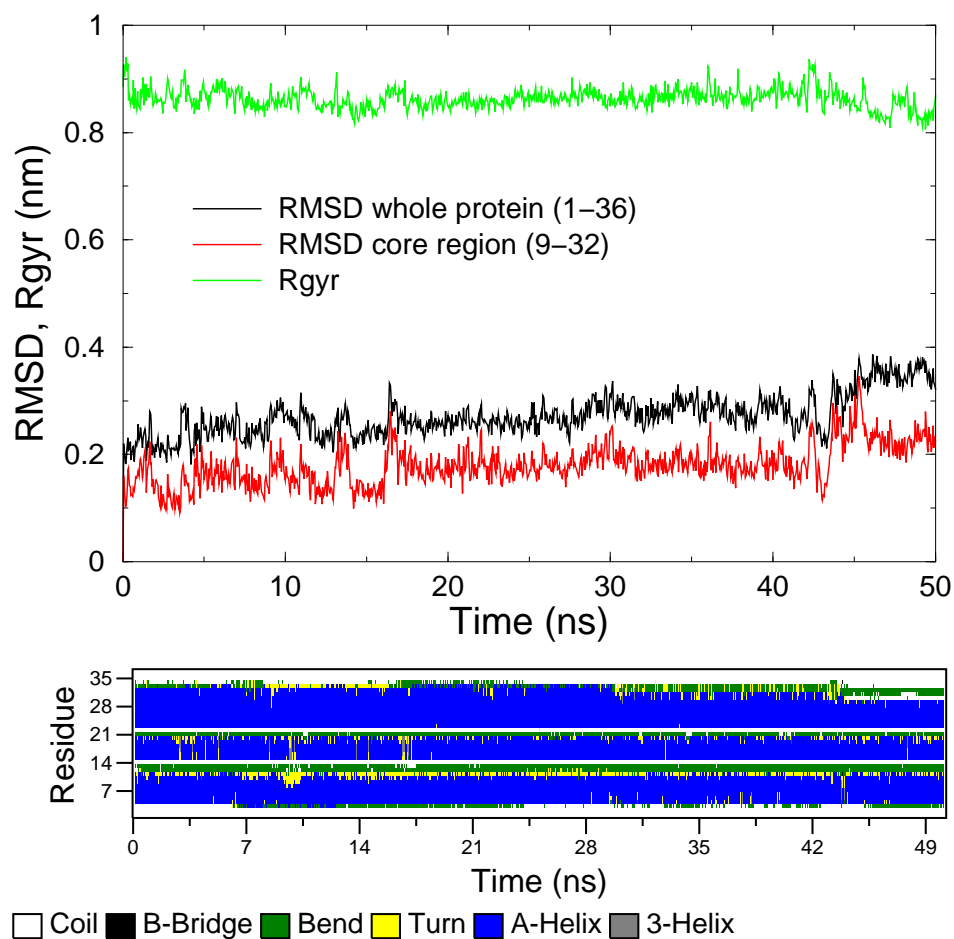


FIG. 2: All-atom MD structural characterization of HP36 native conformation. Top: time evolution of the radius of gyration (green), RMSD of the whole protein (black) and of the core region (red) calculated against the average minimized NMR structure. The core region comprises residues 9–32. Bottom: time evolution of the secondary content (DSSP criterion).

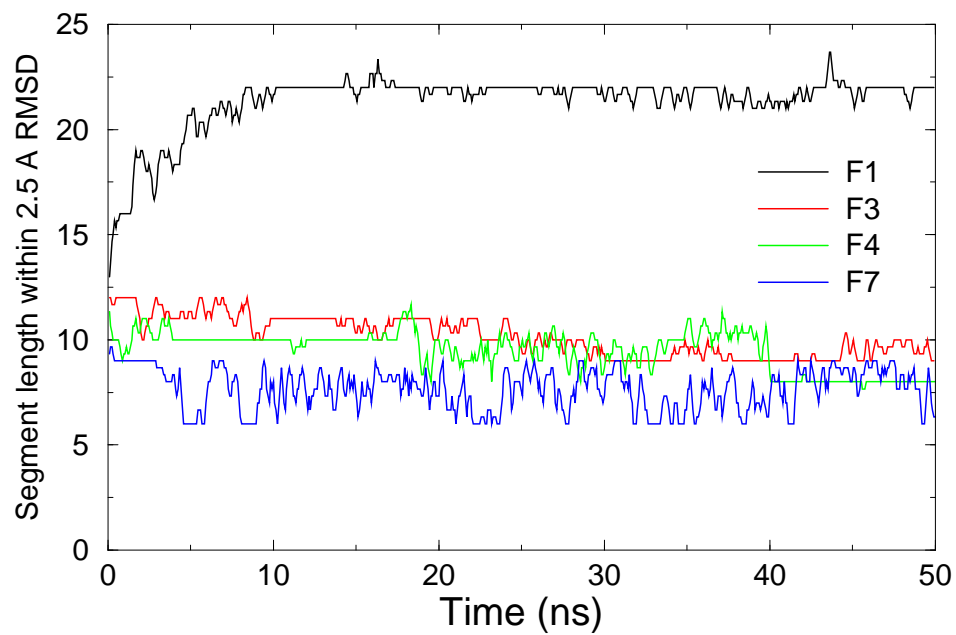


FIG. 3: Time-evolution, during simulations F1, F3, F4 and F7, of the length of the largest protein fragment with an RMSD smaller than  $2.5\text{\AA}$  from the native structure.

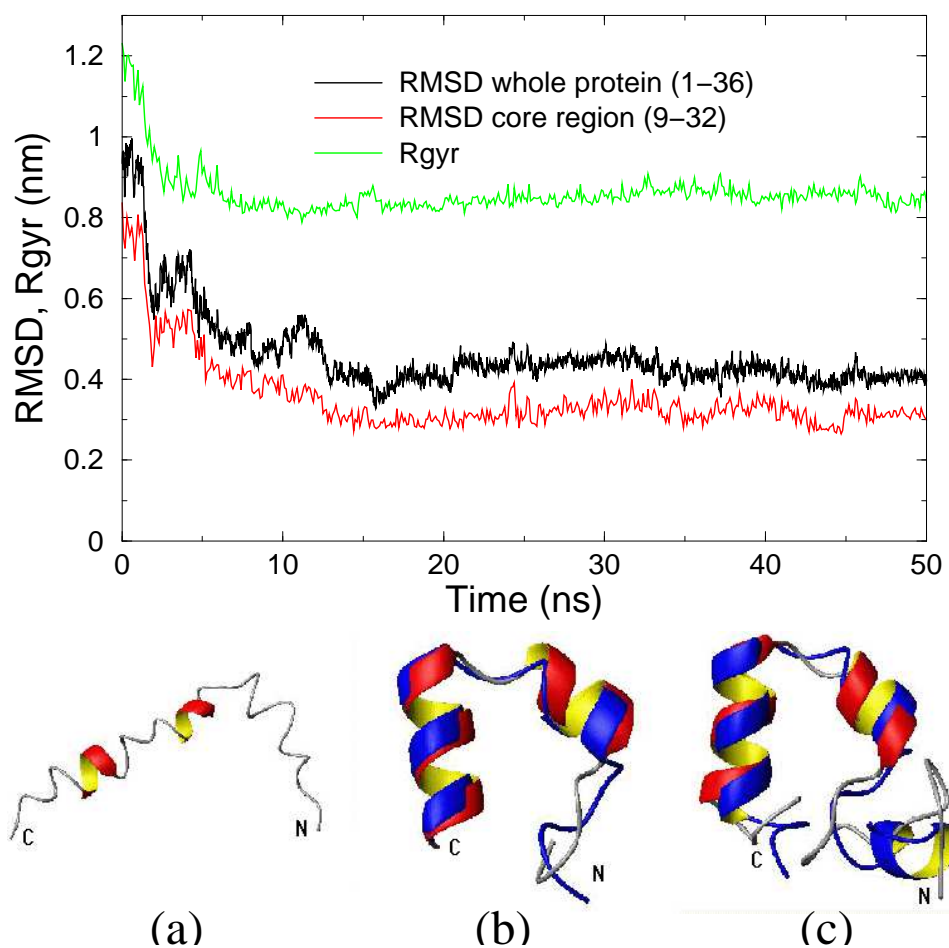


FIG. 4: Top panel: time evolution during simulation F1 of the radius of gyration (green), of the RMSD over the whole protein (black) and over the core region (red). Lower panel: (a) the starting structure of simulation F1; best native structural alignment over the (b) core-region and (c) entire protein of the representative structure of trajectory F1. The representative is colored in red while the native reference conformation is blue.



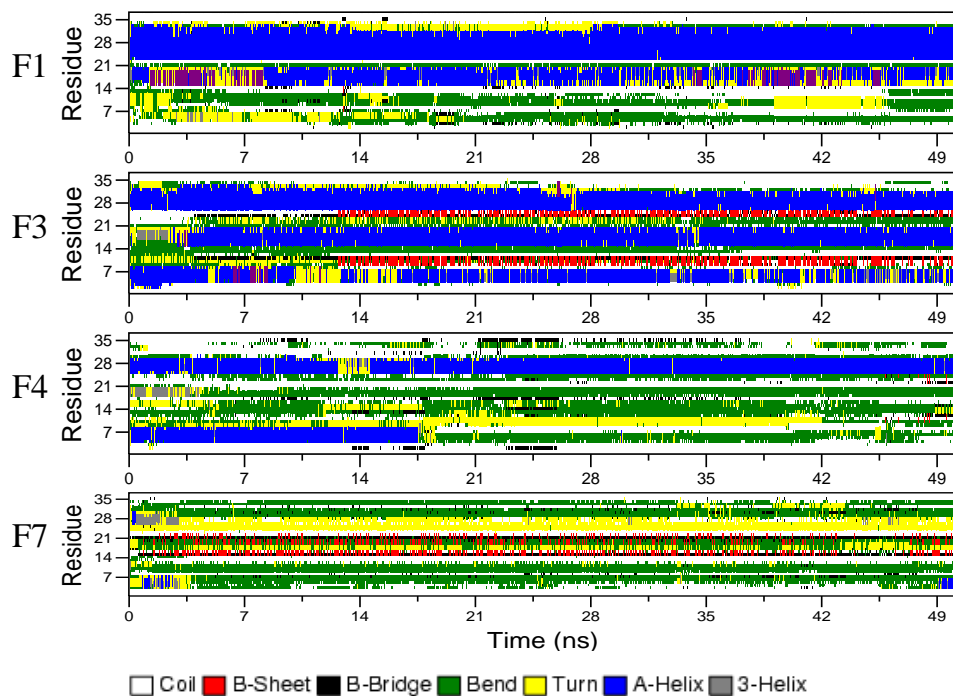


FIG. 5: Secondary structure time evolution for simulations F1, F3, F4 and F7. The DSSP criterion is used to define secondary structure motifs.

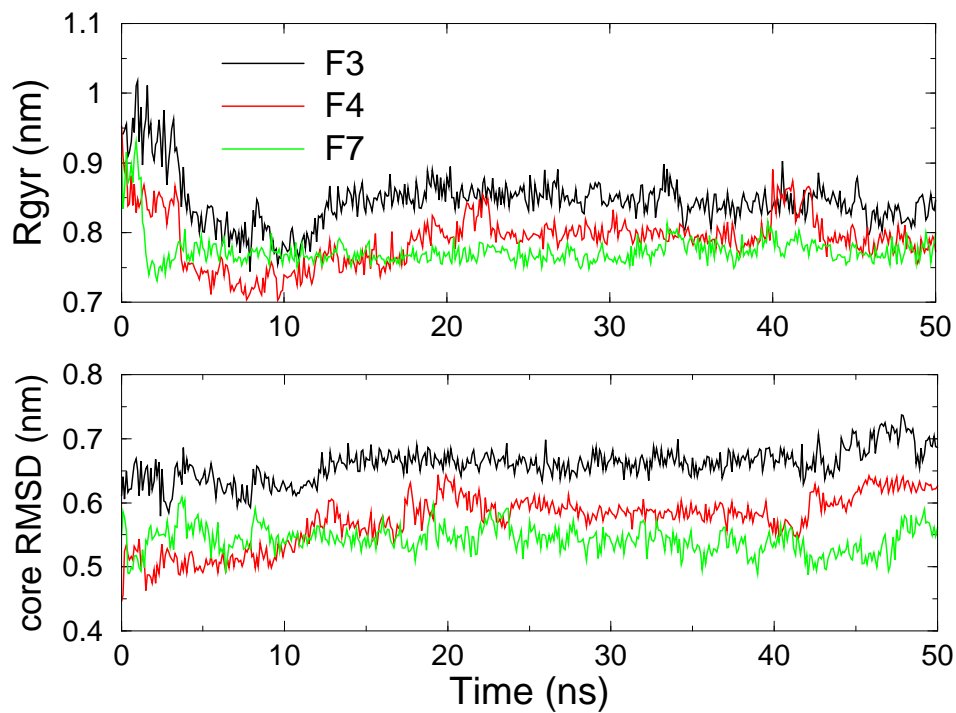


FIG. 6: Time evolution of radius of gyration (top) and core-RMSD (bottom) of HP36. The RMSD was calculated against the average minimized NMR structure of HP36.

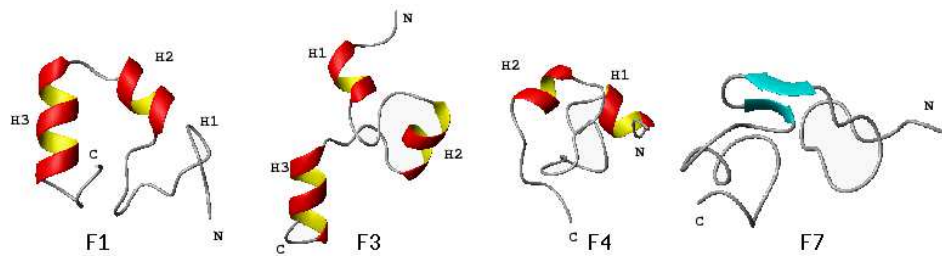


FIG. 7: Representative conformations of the most populated conformational clusters in simulations F1, F3, F4 and F7.

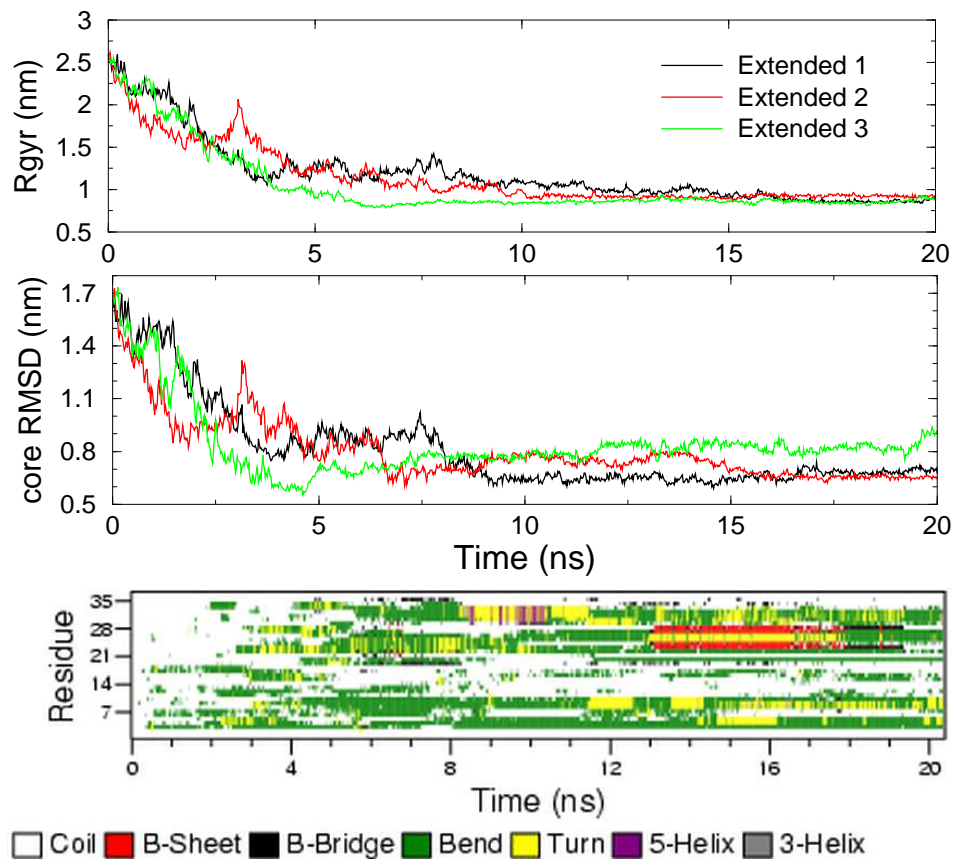


FIG. 8: Time evolution of radius of gyration (top) and core-RMSD (middle) of HP36 in three different runs starting from the fully-extended state. Bottom: typical time evolution of the secondary content during simulations starting from the extended conformation.

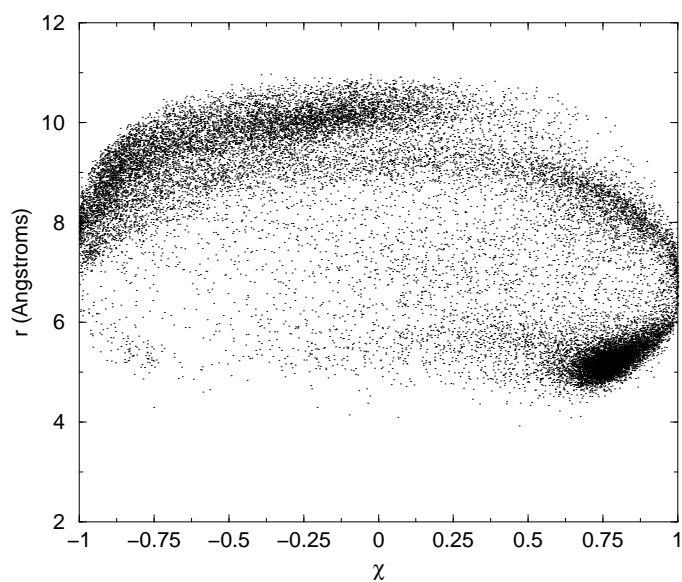


FIG. 9: Scatter plot of the chirality and end-to-end distance of fragments taken from the representative structures of PDBselect.

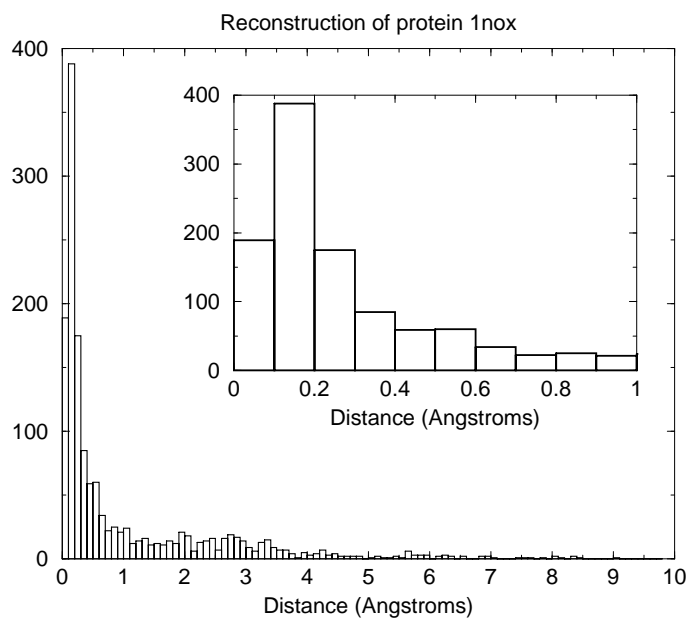


FIG. 10: Histogram for the distance of the reconstructed heavy-atoms from the crystallographic positions in protein 1nox.